Food Chemistry 403 (2023) 134286

Contents lists available at ScienceDirect

Food Chemistry

journal homepage: www.elsevier.com/locate/foodchem

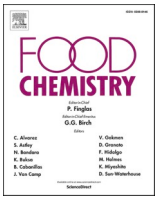

Simultaneous electrochemical detection of antioxidants Hydroquinone, Mono-Tert-butyl hydroquinone and catechol in food and polymer samples using ZnO@MnO_2-rGO nanocomposite as sensing layer

Viyana Movahed [a], Leila Arshadi [b], Mehrnaz Ghanavati [c], Ehsan Mahdavi Nejad [d], Zahra Mohagheghzadeh [e], Mosayeb Rezaei [f,*]

[a] Student Research Committee, Faculty of Pharmacy, Shahid Beheshti University of Medical Sciences, Tehran, Iran
[b] Faculty of Chemistry, Bu-Ali Sina University, Hamedan, Iran
[c] Department of Chemistry, Islamic Azad University, North Tehran Branch, Tehran, Iran
[d] Department of Chemistry, Faculty of Science, Gachsaran Branch, Islamic Azad University, Gachsaran, Iran
[e] Department of Chemistry, Faculty of Sciences, Persian Gulf University, Bushehr, Iran
[f] Knowledge-based Department, Farapol Jam Chemical Industrial, Hamedan, Iran

ARTICLE INFO

Keywords:
Hydroquinone
Mono-Tert-butyl hydroquinone
Catechol
Electrochemical determination

ABSTRACT

A sensing layer containing ZnO@MnO_2-rGO nanocomposite was used for modification glassy carbon electrode (GCE) for monitoring some antioxidant molecules including Hydroquinone (HQ), Mono-Tert-butyl hydroquinone (MTBHQ) and catechol (CC). The resulting ZnO@MnO_2-rGO/GCE exhibited significant electrocatalytic activities toward the electro-oxidation of MTBHQ, HQ, and CC in the linear range (LR) of 0.008 to 10 μM and 10 to 350 μM for MTBHQ, 0.008 to 10 μM and 10 to 320 μM for HQ, 0.008 to 8 μM and 8 to 330 μM for CC with the limits of detection (LOD) of 0.0011, 0.0012 and 0.001 μM, respectively by differential pulse voltammetric (DPV). The prepared sensor has been used to analysis of different real samples containing target analytes with satisfactory results. Based on the percentage of recovery range (95.5–104.4 %), Relative standard deviation (RSD%, below 3.51 %), and the obtained data from the HPLC method, the presented method are accurate with acceptable precision.

1. Introduction

The contemporaneous monitoring of the isomers of molecules is a severe challenge in analytical chemistry because of their similar physical, chemical, and electrochemical properties. For this reason, it is vital to develop a simple, selective, and sensitive method for monitoring them simultaneously.

HQ, MTBHQ, and CC are three isomers of phenolic compounds, that are applied in industrial production of cosmetics, coal-tar production, pharmaceuticals, tanning, pesticides, flavouring agents, polymerization inhibitor and antioxidants, paper manufacturing, chemicals dyes, reducing agent, food and photography and photo stabilizer (Hassan, Hathoot, Abo oura, & Azzem, 2018; Ishack & Lipner, 2022; Sebastian, Yu, Balram, Al-Mubaddel, & Noman, 2022).

Also, these compounds are used in polymer industries because of their excellent antioxidant features, chemical stability, cost-effective, and availability (Ishack & Lipner, 2022; Nogales-Delgado, Guiberteau, & Encinar, 2022; Wang et al., 2022). The antioxidant properties of MTBHQ, HQ, and CC are different due to differences in the position of the –OH groups. The structure of MTBHQ, HQ, and CC are shown in Scheme 1a (Pinnataip & Lee, 2021). Phenolic antioxidants can prevent the unwanted polymerization process in the reactor and blender during the esterification reaction of Unsaturated Polyester Resins (UPS).

In addition to the advantage of HQ, MTBHQ, and CC, they have some disadvantages. Because they are highly toxic and highly stable in the ecological environment, they tend to be widely distributed in the environment and difficult to degrade. The target antioxidants are classified as priority pollutants because high concentrations of these substances cause headaches and cancer, fatigue, kidney damage, and a decrease in liver function. Researchers have proposed two main ways in which phenolic antioxidants play a protective role as follows (Bendary, Francis, Ali, Sarwat, & El Hady, 2013):

* Corresponding author.
E-mail address: Mosayebrezaei@gmail.com (M. Rezaei).

https://doi.org/10.1016/j.foodchem.2022.134286
Received 27 June 2022; Received in revised form 12 September 2022; Accepted 13 September 2022
Available online 17 September 2022

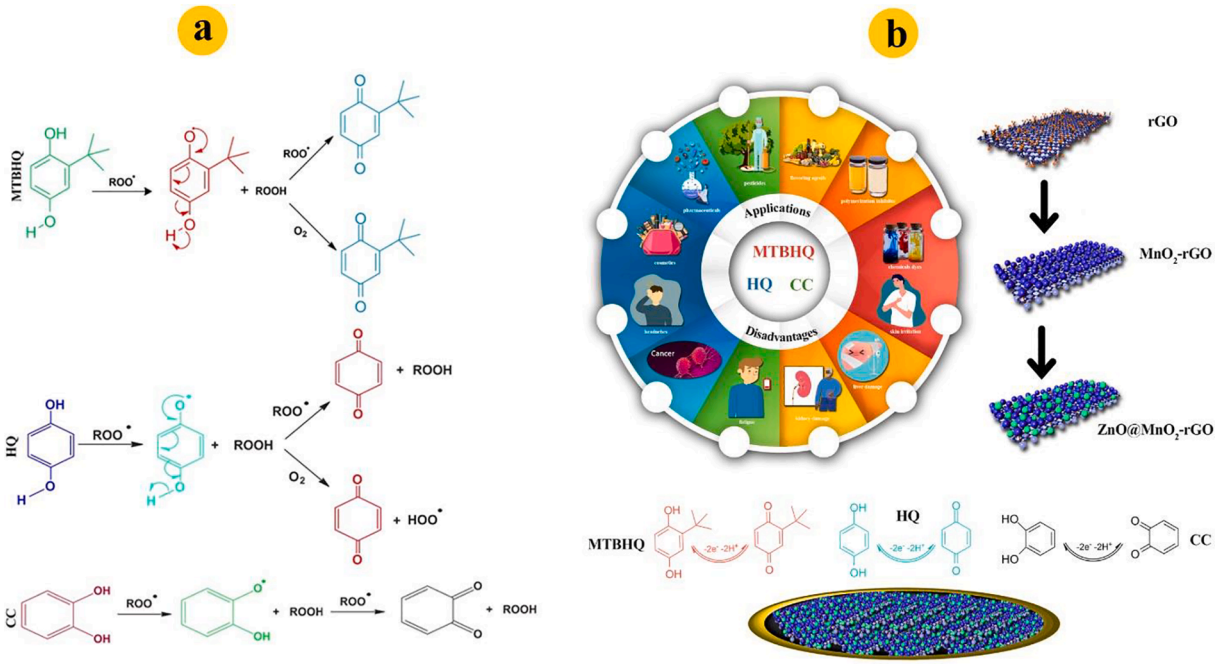

Scheme 1. (a) The structure and the antioxidant mechanisms of MTBHQ, HQ and CC, (b) Application, disadvantages and proposed electro-oxidation of MTBHQ, HQ, and CC.

$R^{\cdot} + HO\text{-}R'\text{-}OH$ c $RH + HO\text{-}R'\text{-}O^{\cdot}$

$R^{\cdot} + HO\text{-}R'\text{-}OH \rightarrow R^{-} + HO\text{-}R'\text{-}O^{\cdot+}$

The path to creating the antioxidant properties of the phenolic compounds is shown in Scheme 1a.

Several techniques of methods including chromatographic-based methods, spectrophotometric-based methods, and electrochemical-based methods have been used to determine the antioxidants. On the one hand, chromatographic-based methods, spectrophotometric-based methods have high accuracy and repeatability, in the other hand, they have some disadvantages such as time-consuming process, sample separation, complex pretreatment, and high cost of instruments (Kathuria, Bhattu, Verma, & Billing, 2022). Alternatively, electrochemical-based methods have been able to attract the attention of analytical chemists due to their accuracy, high sensitivity, selectivity, portability, and simplicity (Afkhami, Madrakian, Sabounchei, Rezaei, Samiee, & Pourshahbaz, 2012; Awang et al., 2021; Bagheri, Afkhami, Khoshsafar, Rezaei, & Shirzadmehr, 2013; Bagheri, Hajian, Rezaei, & Shirzadmehr, 2017; Pajooheshpour et al., 2018).

However, a lot of researchers reported the individual monitoring of MTBHQ, HQ, and CC but the oxidation peaks of them are grievously overlapped or too close to each other into the surface of ordinary electrodes so the simultaneous determination of these compounds is difficult (Balram, Lian, Sebastian, & Rasana, 2021; Fan, Hao, & Kan, 2018; Harshitha et al., 2021; Vishwanath, Swamy, & Vishnumurthy, 2022; Wu, Zhao, Han, Zhao, Zhu, & Cui, 2021).

To overcome the mentioned problems, some material and especially nanoparticles or nanocomposites have been used for modification of common electrodes such as GCE, carbon paste electrode, gold electrode, and others in order to creating the efficient sensing layer (Bagheri, Shirzadmehr, & Rezaei, 2015, 2016; Bagheri, Shirzadmehr, Rezaei, & Khoshsafar, 2018; Khoshsafar, Bagheri, Rezaei, Shirzadmehr, Hajian, & Sepehri, 2016; Mahmoudi, Hajian, Rezaei, Afkhami, Amine, & Bagheri, 2019; Shirzadmehr, Rezaei, Bagheri, & Khoshsafar, 2016). Meanwhile, the adsorption of molecules with similar structures at the surface of the electrode can make the relationship between concentration and signal to be nonlinear.

Based on the previous reports, some nanomaterials can improve resolution between peaks so the simultaneous determination of analytes with the same peak potential can be made possible. Additionally, these nanomaterials can improve the LR and LOD of electrochemical sensors.

The surface properties of nanomaterials including surface area, roughness (as reaction sites), electron distributions, electrical and thermal conductivity, and energetics make nanomaterials a suitable candidate for use in electrochemical sensors because they can enhance electron transfer and interactions of the electrode surface and analytes (Bagheri, Shirzadmehr, Rezaei, & Khoshsafar, 2018; Karimi-Maleh et al., 2022; Rezaei, 2016; Zeinali, Khoshsafar, Rezaei, & Bagheri, 2018).

Due to the wide variety and especial features, carbon-based nanoparticles (CBN) have been used broadly in chemistry. A comparison between carbon atoms in the plane and edges in CBN shows that the reactivity of the edges of carbon atoms is more than at the plane. One of the ways to boost the chemical and physical properties of CBN and achieve new properties is to merge these materials with other NPs such as Metal NPs and Metal oxide NPs (Kant et al., 2022).

ZnO NPs is an *n*-type metal oxide semiconductors with high chemical stability. In addition to ZnO's high isoelectric point, acceptable electrochemical characteristics (electrical conductivity ~ 230 S cm^{-1}), simple and inexpensive synthesis process, and nontoxicity, which make it an ideal semiconductor material for a wide variety of applications (Kalpana & Devi Rajeswari, 2018). ZnO NPs can provide efficient mechanical support and an electron-conducting pathway for the Manganese dioxide (MnO_2) NPs deposited layer because of their chemical stability, mechanical flexibility, and conductivity. Owing to its high specific capacitance (1370 F g^{-1}), low cost, high specific area, high isoelectric point, natural abundance, and environmental compatibility with good electrochemical activity, MnO_2 NPs (p-type semiconductor; Narrow bandgap ~ 1.44 eV) is one of the most talented transition metal oxides for use in the electrical instruments and especially for use in electrochemical sensors (Xiaona Li, Jiang, Li, Li, & Li, 2022).

Since clinical analysis in a clinical laboratory with huge analytical instruments is costly and an exhausting process and it is also not possible to measure the analytes on-site, analytical chemistry scientists are trying to invent new methods with miniaturization and portability ability. As well as being sensitive and accurate, the methods must be capable of

determining a variety of substances with a variety of properties in the real samples. Despite their low cost, portable field-based size, low response time, and high sensitivity, electrochemical sensors are ideally suited for these new applications in clinical chemistry. In addition to being portable and low cost, miniaturized analytical systems can be used in non-laboratory environments to overcome the disadvantages of conventional methods of testing. The advent of nanomaterials allows the replacement of traditional electrochemical with miniaturized electrodes. It is possible to achieve higher response currents, low work potentials, and low interferences with these sensors. It can be noted that this kind of electrochemical sensors have some disadvantages such as mass transport limitations which it has a negative impact on the sensitivity and detection limit. According to the sensing layer used in the presented method, which was made of nanomaterials, it can be loaded on the screen printed electrode to miniaturize the size of the sensor and create portability (W. Zhang, Wang, Luo, Wang, & Lin, 2020).

The electro-oxidations of HQ, MTBHQ, and CC are feasible to its hydroxyl group of benzene ring hard and also the detection of phenolic compounds directly by using bare electrodes does not show a clear redox peak. In the other hand, for simultaneous determination by electrochemical method, a major problem arises with the redox properties of the HQ, MTBHQ, and CC, which are generally overlapped together for the unmodified electrodes (Deng et al., 2022).

Also, the adsorption of organic molecules on solid electrode surfaces is usually unavoidable. The strong adsorption of organic analytes on electrode surfaces can lead to improved sensitivity, but may also result in poor reproducibility for electrochemical detection of organic compounds. The anti-interfere abilities of solid electrodes are usually poor due to the adsorption of organic interferents on electrode surfaces. The competitive adsorption of phenolic isomers on the electrode surface in the mixtures makes the relationship between the voltammetric response and isomers concentration nonlinear (Deng, et al., 2022). In order to overcome these problems, many chemically modified electrodes have been prepared for the measurement of two of the target analytes. These electrodes were modified by different nanomaterials which have some problem such as low repeatability, Limited linear range, high detection limit and the most importantly, the limited use of the modified electrode to measure target analytes in different real samples with various matrices.

In the presented research, for the first time we focused to develop an electrochemical sensor that is made of modified GCEs by ZnO@MnO_2-rGO for determination of three analytes including HQ, MTBHQ, and CC, which cover all of the mentioned disadvantages of previous modified electrode.

The gained data illustrates that, on the surface of ZnO@MnO_2-rGO/GCE the analytes don't have overlap peaks which makes it possible to measure all three analytes at the same time. Also, the sensitivity and selectivity of the method for monitoring HQ, MTBHQ, and CC were remarkable and excellent in compare to previous studies. The DPV technique was applied to optimize the analysis process and obtain the relationship between the electrode responses to the concentration of analytes. The LOD were calculated based on S/N = 3 for MTBHQ, HQ, and CC for the ZnO@MnO_2-rGO/GCE. For investigation of the efficiency of the method in real samples, target analytes were detected in different water samples, oil and polymer samples and recovery data showed the proposed method can be used with high accuracy in quality control laboratories.

2. Experimental section

2.1. Reagents

MTBHQ, HQ, and CC as target analytes Graphene oxide (GO) powder for the synthesis of reduced graphene oxide (rGO), potassium hexacyanoferrate (II) and (III), and sodium borohydride was provided from Sigma-Aldrich and Merck Company all of the chemicals were analytical grade and used without further treatment. Britton-Robinson buffer solution (B-R) was prepared by mixing 0.04 M boric acid, 0.04 M acetic acid, and 0.04 M phosphoric acid, and used to adjust pH value and as a supporting electrolyte. Deionized distilled water (DDW) was used to prepare solutions.

2.2. Instruments

The optimization and determination electrochemical process was done by a Behpajoh potentiostat/galvanostat system (model BHP-2065, Iran) with a conventional three-electrode system, at approximately 25 °C. The Ag/AgCl (Azar electrode, Iran) was selected as the reference electrode, while the platinum wire was chosen as the auxiliary electrode. For investigation of the electrochemical activity, charge transferability, and the surface properties of working electrodes, GCE, rGO/GCE, MnO_2-rGO/GCE, and ZnO@MnO_2-rGO/GCE were selected and for optimization conditions and determination of analytes, ZnO@MnO_2-rGO/GCE was used as the working electrode. The Metrohm pH meter (model 713, Herisau, Switzerland) was used for adjusting the pH values. The nanomaterials structure was investigated by scanning electron microscopy (SEM) with the SEM-EDX, Philips, XL30 (Netherlands), X-ray powder diffraction (XRD) with the 38066 Riva, Via M. Misone, 11/D (TN), Italy, and Fourier transform infrared (FTIR) with Perkin Elmer, Spectrum 100 (USA).

2.3. Synthesis of nanostructures

2.3.1. rGO

Purchased GO was dispersed in DDW to achieve a uniform suspension by the concentration of 1 mg/ml. The excess amount of sodium borohydride (about 3 mL) was added to the suspension while the mixture was stirred for 30 min then the temperature of the mixture has raised to 100 °C and kept constant for 11 h (Hosseini, Bahmaei, & Davallo, 2021).

2.3.2. MnO_2-rGO

The MnO_2-rGO NPs were prepared by a hydrothermal method. For the decorated MnO_2 NPs at the surface of rGO nanosheets, a solution contains 3.2 gr of $MnCl_2{\cdot}4H_2O$ in 150 mL ethylene glycol was prepared. After that, the solution was transferred into a Teflon-lined stainless-steel autoclave and kept in a muffle furnace at 200 °C for 24 h. The obtained material was allowed to cool down to ambient temperature before being centrifuged and then repeatedly washed three times with distilled water. The collected materials were dried in the oven at 100 °C. Then for the calcination of the materials, it was heated up to 600 °C for 6 h (Anantha et al., 2021).

2.3.3. ZnO@MnO_2-rGO

The ZnO@MnO_2-rGO NPs were synthesized by the same method. Firstly, 3.2 g of $MnCl_2{\cdot}4H_2O$, and 6.61 g of $ZnCl_2$ were dissolved in 150 mL ethylene glycol as a solution. After using a Teflon-lined stainless-steel autoclave at 200 °C for 24 h for synthesizing, the materials were cooled and centrifuged. Then it was dried and heated at 600 °C for 6 h (Anantha, et al., 2021).

2.4. Procurement of electrodes and modification

2.4.1. GCE

To prepare the GCE for modification, after clearing and polishing the bare GCE with different sizes of α-Al_2O_3 (1.0, 0.3, and 0.05 μm), it was cleaned with ultrasonic in ethanol/water (30 min; 50:50 V: V) to achieve a mirror-like finish. The electrode then was instantly rinsed with DDW. In order to activate the electrode surface for better modification, the GCE was immersed in an acidic solution containing HNO_3 solution, ethanol, and DDW (1:1:1 V:V:V) for 30 min.

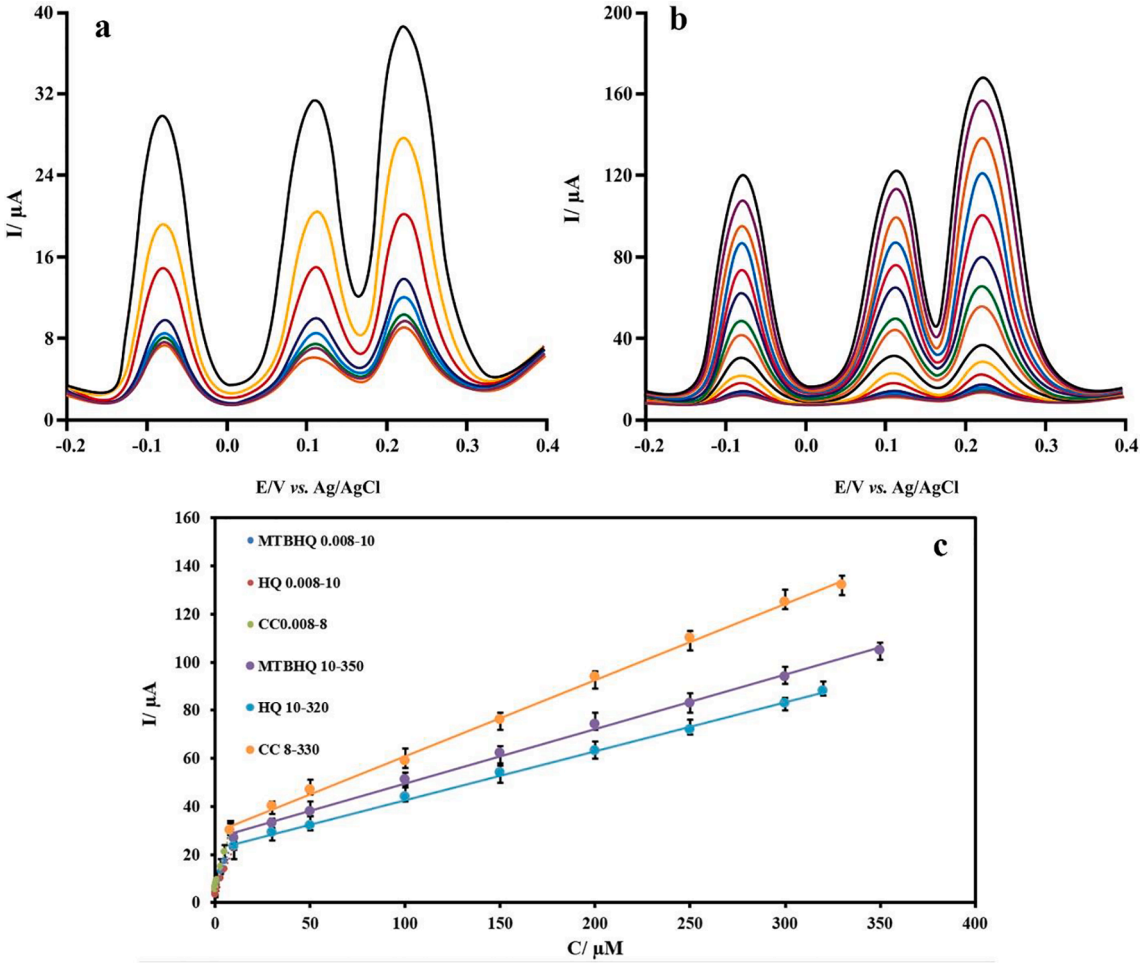

Fig. 1. (a) the XRD patterns and (b) The FTIR spectra of synthesized nanomaterials; SEM image of (c) rGO, (d) MnO_2-rGO, (e) ZnO@MnO_2-rGO nanocomposites, (f) CVs and (g) Nyquist plots of the GCE, rGO/GCE, MnO_2-rGO/GCE, and ZnO@MnO_2-rGO/GCE in 5.0 mM $[Fe(CN)_6]^{3-/4-}$ and 1.0 M KCl.

2.4.2. *Fabrication of working electrodes*

In order to construct modified electrodes including rGO/GCE, MnO_2-rGO/GCE, and ZnO@MnO_2-rGO/GCE, for optimization of the analysis condition and comparing the effect of modifiers, 10 µL of aqueous suspension (rGO, MnO_2-rGO, and ZnO@MnO_2-rGO nanocomposites, respectively) with the concentration of 1 mg/ml were dropped on the surface of activated GCE and dried at room temperature.

2.5. *HPLC detection conditions in experiments*

For the investigation of accuracy, the experimental data of the method were compared to HPLC data with the following condition: The injection volume: 20 µL; the column temperature: 30 °C; Pumping speed: 30 L/min; Wavelength of UV detector: 280 nm for MTBHQ, 300 nm for HQ, 270 nm for CC; Mobile phase solution: methanol–acetonitrile (1:1); Column: C18 (250 × 4.6 mm × 5 µm).

2.6. *Treatment of real samples and spiked sample*

Soybean oil sample: In a 100 mL Erlenmeyer flask, 5 mg of an edible oil sample was dissolved in 5 mL of pure methanol. It had been shaken vigorously for 20 min, then for 15 min, and the mixture was centrifuged at 4000 rpm. Five minutes after the extracts settled, they were quantitatively transferred into a 25 mL volumetric flask. Two times extraction was performed., then collected all extracts, were transferred to the volumetric flask; and then diluted with pure methanol, and kept refrigerated for analysis (Tang et al., 2022).

Water sample: the tap water and river water (from the Karun river, Ahvaz, Iran) samples were collected and without any pretreatment used for analysis.

Orange juice: Firstly, Whatman filter paper was used to filter the orange juice sample. The extract of fruits was filtered through commonly employed Whatman filter paper, then it was transferred into the electrochemical cell (Buledi et al., 2020).

Polymer sample: For analysis, the polymer samples, Unsaturated polyester resin based on Isophthalic acid (I 211), orthophthalic unsaturated polyester resin (O 115), and vinyl ester resin (V 301) were prepared from *Farapol Jam chemical industries Company*. The I 211 and O 115 were cured with the addition of 1 % Cobalt Octoate (1 % in styrene), and 1 % AKPEROX A60 as the catalyst, while the V 301 resin sample was cured with the addition of 1 % Cobalt Octoate (1 % in styrene), 0.5 % Dimethyl aniline (10 % in styrene) and 1 % AKPEROX A60 as the catalyst. During the post-cure process, after 24 h, the I 211 and O 115 cured samples were placed in the oven at 80 ℃ for 3 h. On the other hand, the cured V 301 resin was placed in the oven at 80 ℃ for 2 h and 1 h at 120 ℃. The polymer post-cured samples were cut up into pieces of approximately 0.1 to 0.5 g and placed in a flask for 40 min with 50 mL DDW, which was kept at 70 ℃. Following that, the mixture obtained was cooled to laboratory temperature and filtered. The previous step was repeated three times for each sample. To analyze the obtained sample, 10.0 mL were poured into a 25 mL volumetric flask and diluted with B-R buffer solution pH = 7.0 (Movahed, Rezaei, & Mohagheghzadeh, 2021).

3. Results and discussion

Structure investigation of the synthesized nanomaterial including GO, rGO, MnO_2-rGO, and ZnO@MnO_2-rGO NPs were done by XRD, FTIR, and SEM methods.

3.1. XRD analysis

The XRD pattern of GO, rGO, MnO_2-rGO, and ZnO@MnO_2-rGO nanomaterials is illustrated in Fig. 1a.

There is a typical peak at $2\theta = 10.87^\circ$ (0 0 1) for GO and 26.04° (0 0 2) and 42.53° (0 0 1) in the XRD patterns of rGO, which is a reflection of exfoliated graphite and agrees with previous studies. In conclusion, it appears that $NaBH_4$ converts GO to rGO. The diffraction peaks of the MnO_2-rGO represent the peaks at 16.00°, 25.37°, 28.33°, 32.29°, 34.01°, 37.17°, 40.48°, 42.55°, 43.99°, 48.93°, 56.48°, and 65.42°, which confirms that rGO nanosheets have been loaded with MnO_2 NPs, as indicated by this observation (Kumar, Gajraj, Rameshbabu, Mangalaraja, Joshi, & Priyadarshi, 2022; Vedpathak, Desai, Bhagwat, & Sartale, 2022; Zhao, Ma, Qiao, Fan, Qin, & Shao, 2022). The XRD pattern of ZnO@MnO_2-rGO nanocomposite showed several peaks at degrees of 31.72° (1 0 0), 34.22° (0 0 2), 36.23° (1 0 1), 47.52° (1 0 2), 56.62° (1 1 0), 62.84° (1 0 3), 67.95° (1 1 2), 69.10° (2 0 1), and 77.12° (2 0 2), which were well matched with data of JCPDS-01-078-4498. All four samples are found without obvious impurities (Li et al., 2014).

3.2. FTIR analysis

The FTIR spectra of GO, rGO, MnO_2-rGO, and ZnO@MnO_2-rGO NPs were examined for further investigation, and they are shown in Fig. 1b.

There are some peaks in the FTIR spectrum of GO at 3416.67, 2927.45, 1705.34, 1634.89, 1394.05, and 1254.69 cm^{-1}, which are related to O—H stretching, C—H stretching, C—O—H vibrations, C—O stretching related to phenolic groups, and C═C stretching related to aromatic rings, respectively. When the GO was reduced by $NaBH_4$, the peak related to the oxygen functional group was removed or observed at a very low intensity. It showed two peaks at 1572.19 and 1209.45 cm^{-1} related to C═C and C-OH stretching. By decorating the MnO_2 NPs on the surface of rGO, a new peak was observed at 527.43 cm^{-1} for Mn-O of MnO_2 NPs.

In the FTIR spectrum of ZnO@MnO_2-rGO NPs, Zn-O would be characterized by its stretching vibration at 503.09 cm^{-1} and by its characteristic band at 1036.75 cm^{-1}. A peak between 995 and 1095 cm^{-1}, and a band between 517 and 617 cm^{-1} in an FTIR spectrum, can be attributed to MnO-O vibrations being strained. Therefore, it can be said that the presence of ZnO and MnO_2 NPs was presented on ZnO@MnO_2-rGO NPs.

3.3. SEM image

An analysis of the surface topography of rGO, MnO_2-rGO, and ZnO@MnO_2-rGO NPs was performed using SEM images. Taking SEM images will also ascertain momentous details about the composition and particle size of materials (Fig. 1c-e).

In SEM images of rGO nanosheets, similar thin sheets are observed randomly aggregated with distinct edges, wrinkled surfaces, and folding. The dimension of the mean sheet is approximately 30 × 15 μm. By doping the MnO_2 NPs on the surface of the rGO nanosheet, the morphology has been changed and sheets of rGO were uniformly dotted with NPs with average sizes of 30 nm (Fig. 1d). The ZnO@MnO_2-rGO NPs surface morphology can be seen in Fig. 1e. There is uniform loading of spherical ZnO@MnO_2 NPs and nano-sized particles are attached to rGO's surface. The diameter of the ZnO-MnO_2 nanocomposite was determined 40 nm.

3.4. Investigation of electrochemical properties of the electrodes

The cyclic voltammetry and electrochemical impedance spectroscopy (EIS) techniques were applied in 0.2 M KCl as electrolyte and a redox probe of 5.0 mM $[Fe(CN)_6]^{3-/4-}$ as a redox probe for electrochemical investigation (conductive nature and electrochemical characteristics) of different prepared working electrodes.

Fig. 1f depicts the CVs of at GCE, rGO/GCE, MnO_2-rGO/GCE, and ZnO@MnO_2-rGO/GCE in the presence of the redox probe. The peak current (Ip) and peak potential separation (ΔEp) have changed with the modification of sensing layers by rGO, MnO_2-rGO, and ZnO@MnO_2-rGO.

At the surface of bare GCE, the electrochemical probe represents a weak reversible CV peak (Ipa = 52 μA, Ipc = 30 μA) with high ΔEp (170 mV). ΔEp has decreased and Ip has increased while rGO has been used to modify the GCE surface (Ip = 71 μA, ΔEp = 162). It can be due to two-dimensional structure of rGO which lead to high theoretical surface area, and also with reduction of OH fuctional groups at the surface and in the edges of rGO the electron transfer pathway have increased significantly, so the conductivity of the modified electrode has improved.

MnO_2-rGO nanoparticles possessing a high conductivity were found to be well-defined peaks on the surface of MnO_2-rGO/GCE, resulting in a higher Ipa (106 μA) and a lower ΔEp (122 mV) value in comparison to GCE and rGO/GCE, further ameliorating the conductivity and reversibility of the modified electrode. By doping rGO with nanomaterials, you can create economical sensors with practical properties while improving their electronic and chemical characteristics. Also, based on previous report, the MnO_2-rGO composite has a higher conductivity compared with pure MnO_2 NPs and rGO. In the other hand by doping the MnO_2 NPs to the surface of rGO the surface area of prepared nanocomposite has increased significantly and the results obtained in this experiment can be justified (Zhang et al., 2016).

Furthermore, when GCE was modified with ZnO@MnO_2-rGO, the highest Ip (Ipa = 163 μA, Ipc = 122 μA) and the lowest ΔEp (100 mV) were obtained, which can be attributed to the synergistic effect between ZnO@MnO_2 nanocomposite and rGO nanosheets, which enhanced the catalytic ability, the electron transfer rate, and the conductivity. By adding the ZnO NPs to the MnO_2-rGO nanocomposite the synergism between the three materials improved the performance of electrochemical properties. Addtition of ZnO NPs to the MnO_2-rGO nanocomposite may be lead to increasing the electrochemical active surface area and the improved electrode performance (Wi et al., 2015).

The EIS analysis was applied to analyze the surface properties and the charge transferability of the electrodes and the Nyquist plot for the electrodes is shown in Fig. 1g. The Rct values were obtained at 468, 371, 172, and 106 Ω for the bare GCE, rGO/GCE, MnO_2-rGO/GCE, and ZnO@MnO_2-rGO/GCE, respectively. Because the rGO sheets increase the surface area of GCE, it can improve the number of electrochemical reaction sites, so the Rct has decreased by using the rGO/GCE as the working electrode from 468 for GCE to 371 Ω. By placing the MnO_2 NPs on the surface of rGO nanosheets and increasing the conductivity, the electron transfer resistance for MnO_2-rGO/GCE was obtained (172 Ω) lower than rGO/GCE. This result confirms that the electron transfer rate was considerably increased at the surface of MnO_2-rGO/GCE. The ZnO@MnO_2-rGO/GCE has the lowest Rct (106 Ω) out of all electrodes tested because of its high conductivity, its vast surface area, and its unique catalytic properties, making it the best candidate to use in electrochemical applications in this research. It can be seen that the CV data and the gained data from EIS analysis confirm each other.

3.5. Voltammetric response of MTBHQ, HQ, and CC at the differently working electrodes

Fig. 1S a and b represents the DPVs and CVs of the activated GCE, rGO/GCE, MnO_2-rGO/GCE, and ZnO@MnO_2-rGO/GCE in B-R buffer

solution (0.2 M, pH 7.0). In DPVs analysis, three oxidation peaks can be observed by different oxidation currents (Ip) and potentials (Ep) between −200 and +400 V using the four modified electrodes, and this can be attributed to the 10, 10 and 8 μM HQ, MTBHQ and CC redox reaction (Fig. 1S a). For the activated GCE, the two broad overlapped oxidation peaks of MTBHQ, HQ, and CC with weak intensities are located at about −0.05 and 0.1–0.3 V, respectively. At the surface of the other electrodes, three well-separated oxidation peaks were observed, while the Ip and Ep have changed as follows:

Ip: rGO/GCE < MnO_2-rGO/GCE < ZnO@MnO_2-rGO/GCE

Ep: rGO/GCE > MnO_2-rGO/GCE > ZnO@MnO_2-rGO/GCE

Owning to highest electrochemical responses, MTBHQ, HQ, and CC exhibit the best sensitivity at ZnO@MnO_2-rGO/GCE in comparison to other electrodes. The oxidation peak potentials for MTBHQ, HQ and CC were observed in −0.08, 0.11, and 0.21 mV, respectively, with a peak-to-peak separation of 190 (for MTBHQ-HQ) and 100 (HQ-CC) mV. So, MTBHQ, HQ, and CC could be determined simultaneously by the DPV technique because the peak-to-peak separations were large enough.

Due to their small size and large coverage of corner and edge sites, the NPs have different physicochemical properties from their bulk, metal oxide nanoparticles can be used in the electroanalysis of analytes. A reduction in particle size causes three main changes: Firstly, structural changes, whereby the lattice symmetry and cell parameters could be altered, even resulting in nonstoichiometric. Secondly, the electronic properties of the metal oxides in the nanoparticulate form can also be changed, due to the quantum confinement effect. Thirdly the surface properties of the metal oxides, whereby the band gap is drastically increased in nanoparticles, leading to a change in conductivity and chemical reactivity. Due to the different structure of the target analytes and also their different interaction with the used oxide nanoparticles and also the mentioned features the modified electrod can separat of overlapped peaks. Also, the mentioned reasons are the reason for the difference in the position of the peaks on the surface of different electrodes (George, Antony, & Mathew, 2018; Ratnam, Manjunatha, Janardan, Naidu, & Ramesh, 2020).

The CV technique was also applied to investigate the behavior of the 5 μM HQ, MTBHQ and CC on the electrode surface and the voltammograms were shown in Fig. 1S b-d. In contrast to GCE which showed a quasi-reversible voltammogram for analytes, reversible peaks were obtained in the individual determination of MTBHQ, HQ, and CC at the surface of rGO/GCE, MnO_2-rGO/GCE, and ZnO@MnO_2-rGO/GCE. An individual determination of MTBHQ has an oxidation currents of 1.26, 5.08, 7.56, and 12.03 μA, at the GCE, rGO/GCE, MnO_2-rGO/GCE, and ZnO@MnO_2-rGO/GCE, with a peak-to-peak separation of 138, 101, 71 and 59 mV respectively. Oxidation peaks of HQ and CC have appeared in 139 (Ipa = 2.23 μA), 125 (Ipa = 7.18 μA), 114 (Ipa = 13.25 μA), and 108 (Ipa = 20.14 μA) mV (for HQ), and 253 (Ipa = 2.09 μA), 227 (Ipa = 5.62 μA), 218 (Ipa = 11.51 μA), and 209 (Ipa = 17.36 μA) mV (for CC) at the GCE, rGO/GCE, MnO_2-rGO/GCE, and ZnO@MnO_2-rGO/GCE, respectively. It can be seen that by modification of GCE the oxidation peak potentials have shifted to the left side which demonstrated that the oxidation of three analytes was easier at these electrodes and the best result has occurred at ZnO@MnO_2-rGO/GCE.

This betterment in electron transfer kinetics can be due to the two factors. Firstly, ZnO, MnO_2, and the composite of them have been shown to enhance the oxidation process of MTBHQ, HQ, and CC significantly as they have nano-size with large active surface area, high loadings, and high electro-catalytic activity. As a result, it reduces the charge transfer resistance, increasing reversibility and improving peak currents. Furthermore, rGO nanosheets exhibit excellent properties in the planar direction, including high surface area per unit volume, ability to decorate the nanomaterials on it, and thermal conductivity. So, it can introduce new special properties for nanocomposite and provide current density for modified electrodes. Because the decorated rGO with ZnO and MnO_2 NPs formed a 3D structure, the ZnO, and MnO_2 NPs impressively inhibited the stacking of individual rGO units and thereby enhanced the utilization of rGO-based nanocomposites. As a result, improving the electrochemical performance for the measurement of MTBHQ, HQ, and CC in electro-analytical applications.

3.6. Selection of optimum pH value and supporting electrolyte

The effect of supporting electrolyte and pH values on the electrochemical response of 30 μM MTBHQ, HQ, and CC, at the surface of ZnO@MnO_2-rGO/GCE, was investigated by DPVs.

The voltammograms and plot of Ip and Ep versus pH are plotted in Fig. 1S e. Based on Fig. 1S f-h, it is concluded that the maximum responses of the electrode for oxidation of MTBHQ, HQ, and CC were obtained when the pHs have increased from 4.0 to 7.0, and then decrease when the pHs were increased further.

The pKa values of MTBHQ, HQ and CC are 10.80, 9.85, and 9.40, respectively. Since MTBHQ, HQ, and CC is three protic aromatic molecules, which could effortlessly generate deprotonation and turn into anion forms. At the pH range below 7.0, when the pH values have increased from 4.0 to 7.0, the analytes have protonated in the form of $^{2+}$HO-R-OH^{2+}, so the oxidation peak currents have enhanced, significantly. In contrast, whereas pHs have changed between 7.0 and 9.0 the –OH- ions have been increased and the adsorption of the analyte might be decreased from the bulk solution onto the working electrode surface. Therefore, the oxidation currents decreased at a pH higher than 7.0. Also, the analytes can be rapidly oxidized in the air when the pH values were more than 7.0. Finally, to achieve the best sensitivity, pH = 7.0 has been selected for the measurement of MTBHQ, HQ, and CC in further experiments (Deng, et al., 2022; Karthika, Raja, Karuppasamy, Suganthi, & Rajarajan, 2020; Park, Kim, Min, & Choi, 2022).

Also, Fig. 1S f-h illustrates the Eps for the oxidation of MTBHQ, HQ and CC negatively repositioned with heightening the pH values. The relationships between the Eps of MTBHQ, HQ, and CC versus pH values were also perused. For MTBHQ, HQ, and CC the linear regression equations for Eps versus pH could be expressed as Ep = -0.0548pH + 0.3065 (R^2 = 0.9938), Ep = -0.0556pH + 0.505 (R^2 = 0.9954) and Ep = -0.0616pH + 0.6444 (R^2 = 0.9957), respectively. According Nernst equation, if slope of relationship between peak potential and pH in linear regression equations was about −0.059 V/pH at 25∘C, the electrochemical processes of each molecule involving the same number of protons and electrons. Based on the obtained slopes for the analytes and comparison with the Nernst equation, it can be concluded that the number of protons and electrons involved in the electrochemical oxidation process of MTBHQ, HQ, and CC are equal.

It is well known that the supporting electrolyte is used to increase the conductivity of the solution, reduce the Ohmic drop effect, eliminate the migration of electroactive species towards the electrodes through electrostatic attractions, and maintain a constant ionic strength and pH. Additionally, the type of electrolyte and the pH of the electrolyte can have a significant impact on the peak current, peak potential, and peak shape of an electroactive organic compound (Sipa, Brycht, & Skrzypek, 2018).

Thus, the effect of various supporting electrolytes such as KNO_3, acetate buffer solution, B-R universal buffer, and phosphate buffer solution on electrochemical responses of the analytes, was checked. In consequence, the maximum electrochemical responses, the well-defined oxidation peak shapes and the lowest background current for oxidation of the three analytes were obtained when 0.1 M B-R buffer solution was applied as the supporting electrolyte. As a result, B-R universal buffer has a greater conductivity than the other investigated buffers solution because it contains phosphate acid, boric acid, acetic acid and sodium hydroxide (Rosida, Mulyasuryani, & Tjahjanto, 2017).

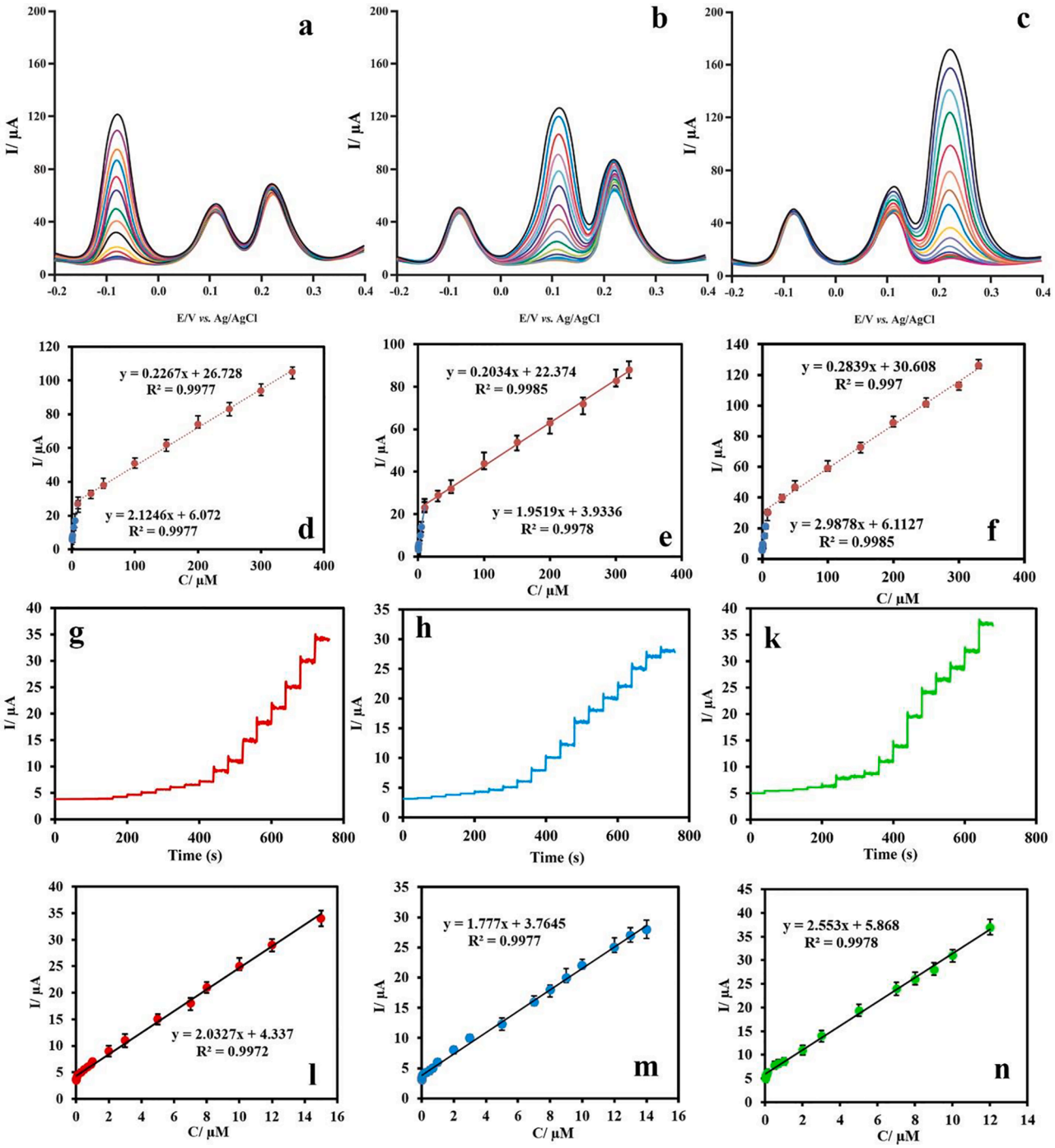

Fig. 2. DPVs of individual determination of (a) MTBHQ, (b) HQ, and (c) CC at ZnO@MnO_2-rGO/GCE in B-R buffer solution pH = 7; The calibration plots (d) MTBHQ, (e) HQ, and (f) CC; Amperometric detection of (g) MTBHQ, (h) HQ, and (k) CC at ZnO@MnO_2-rGO/GCE in B-R buffer solution at 120 rpm with pH = 7 at fixed potentials of −0.08, 0.11, and 0.21 V; The amperometric calibration plots (l) MTBHQ, (m) HQ, and (n) CC.

3.7. The effect of sweep rate on electrochemical signals

The CV technique was used to study the influence of scan rates when changed between 25 and 300 mV/s on the electro-oxidation of 5 µM of MTBHQ, HQ, and CC using ZnO@MnO_2-rGO/GCE (Fig. 2S a, e, and i). The CVs for MTBHQ, HQ, and CC illustrate reversible processes in that the redox peak currents were improved while the Ep oxidation shifted in a positive direction when the scan rates increased from 25 to 300 mV/s. The oxidation signals have changed linearly with the square root of scan rates for MTBHQ, HQ and CC with the linear regression equations of Ipa = 1.2004 $\sqrt{v}$ − 0.8922 (R^2 = 0.9971), Ip = 1.0911$\sqrt{v}$ − 0.9176 (R^2 = 0.9931) and Ip = 1.7865$\sqrt{v}$ − 1.2097 (R^2 = 0.9979), respectively. Based on these experiments, it is found that MTBHQ, HQ, and CC were diffusion-controlled rather than surface-controlled at the surface of ZnO@MnO_2-rGO/GCE (Fig. 2S b, g and j).

In the other calculation, the Semerano coefficient was computed by plotting the Log Ipa versus Log the scan rates and determining the slop (Fig. 2S c, f, and k). Ideally, when the Semerano coefficient was equal to 0.5, the electrochemical process at the surface of ZnO@MnO_2-rGO/GCE was diffusion-controlled, and while the coefficient was equal to 1 the electrochemical surface process was adsorption controlled. The Log Ipa dependence of Log the scan rates for MTBHQ, HQ and CC was described

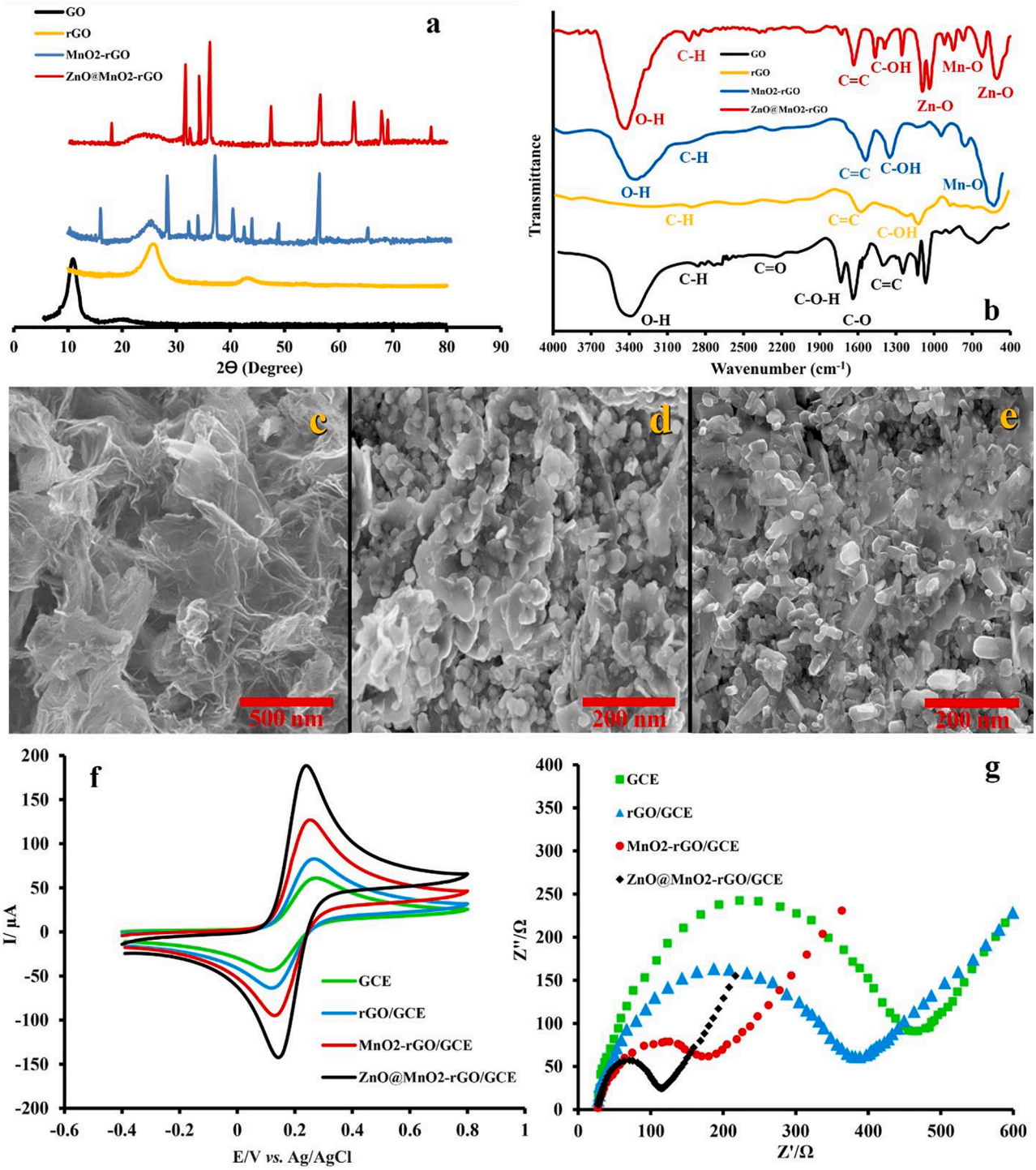

Fig. 3. DPVs of simultaneous detection of MTBHQ, HQ, and CC at ZnO@MnO_2-rGO/GCE in the range of (a) 0.008 to µM for MTBHQ, 0.008 to 10 µM for HQ, 0.008 to 8 µM for CC; (b) 10 to 350 µM for MTBHQ, 10 to 320 µM for HQ, 8 to 330 µM for CC; (c) Calibration plots of simultaneous detection.

as Log Ipa = 0.5325 log v − 0.0213 (R^2 = 0.9973), Log Ipa = 0.5353 Log v − 0.0729 (R^2 = 0.9951), Log Ipa = 0.544 Log v + 0.1295 (R^2 = 0.9968), respectively. The slope of three analytes 0.5325, 0.5353, and 0.5440 for MTBHQ, HQ, and CC were close to the Semerano coefficient theoretical value of 0.5 Log Ipa/Log v at 25 ∘C, suggesting that the electrochemical process of oxidation of MTBHQ, HQ, and CC were a diffusion-controlled.

Fig. 2S d, h and l also shows that with an increase in the scan rate, the peak potentials for oxidation and reduction have shifted in positive and negative directions, respectively. According to these results, electrochemical reactions become less reversible with increasing scan rates. The electrochemical behaviour of three analytes can be investigated by linearly relating anodic (Epa) or cathodic peak potentials (Epc) to the natural logarithm of scan rates (lnv) at scan rates between 100 and 300 mV/s. In general, the relationship between the Epa/Epc and scan rate (v) is described as the following equations:

$$\text{Epa} - \text{v}\, Epa = E0 + \left[\frac{RT}{(1-\alpha)nF}\right] Lnv \quad (1)$$

$$Epc - vEpc = E0 + \left[\frac{RT}{anF}\right] Lnv \quad (2)$$

E^0 = Formal redox potential, R = Molar gas constant, T = Thermodynamic temperature,

α = Electron transfer coefficient, n = Electron transfer number, F = Faraday's constant.

The regression equations for MTBHQ, HQ and CC were as below:

MTBHQ

Oxidation Epa = 0.0221Lnv − 0.1831 R^2 = 0.9974 Eq.3

Reduction Epc = −0.0212Lnv − 0.0482 R^2 = 0.9972 Eq.4

HQ

Oxidation Epa = 0.0213Lnv + 0.0148 R^2 = 0.9913 Eq.5

Reduction Epc = −0.0206Lnv + 0.1499 R^2 = 0.9984 Eq.6

CC

Oxidation Epa = 0.0233xLnv + 0.1156 R^2 = 0.998 Eq.7

Reduction Epc = −0.0219Lnv + 0.2732 R^2 = 0.9947 Eq.8

Based on gained slopes the n value involved in the electro-oxidation process of MTBHQ, HQ and CC can be calculated to be approximately 2.37, 2.45 and 2.28, which all of them were close to 2. According to the pH investigation of electro-oxidation of the analytes and obtained results in this section it can be concluded that the electrochemical reaction of the analytes at ZnO@MnO_2-rGO/GCE was a two-electron and two-proton process which is well consistent with that reported previously. The proposed mechanism of surface reaction were presented in scheme 1b.

3.8. Electrochemical monitoring of MTBHQ, HQ, and CC

3.8.1. Individual detection

In the individual voltammetric determination of each analyte at ZnO@MnO_2-rGO/GCE, the concentration of two analytes remain constant while the other analyte has changed linearly from 0.008 to 10 and 10 to 350 μM for MTBHQ, from 0.008 to 10 and 10 to 320 μM for HQ, from 0.008 to 8 and 8 to 330 μM for CC. The calibration curves for the individual measurement of MTBHQ, HQ, and CC were plotted in Fig. 2a-c.

It can be seen that by increasing the concentration of each analytes, the Epa of them remained unchanged. In the other hand, the obtained signal for electro-oxidation of MTBHQ, HQ and CC were increased, and the linear regression equation were Ipa = 2.1246C + 6.072 (R^2 = 0.9977, 0.008 to 10 μM), and Ipa = 0.2267C + 26.728 (R^2 = 0.9977, 10 to 350 μM) for MTBHQ, Ipa = 1.9519C + 3.9336 (R^2 = 0.9978, 0.008 to 10 μM) and Ipa = 0.2034C + 22.374 (R^2 = 0.9985, 10 to 320 μM) for HQ, Ipa = 2.9878C + 6.1127 (R^2 = 0.9985, 0.008 to 8 μM) and Ipa = 0.2839C + 30.608 (R^2 = 0.997, 8 to 330 μM) for CC (Fig. 2 d-f).

3.8.2. Amperometric detection of analytes

MTBHQ, HQ, and CC concentrations were also determined by the amperometric method (Fig. 2g-k) by stirring the B-R buffer solution at 120 rpm with pH = 7 for the duration of the experiment and recording MTBHQ, HQ, and CC oxidation currents at fixed potentials of −0.08, 0.11, and 0.21 V, respectively. Fig. 2 l- n represent the amperometric currents vs time response of the ZnO@MnO_2-rGO/GCE for the determination of MTBHQ, HQ, and CC, respectively. The ZnO@MnO_2-rGO/GCE displayed a linear response to MTBHQ, HQ and CC in the concentration range of 0.008–13, 0.01–14 and 0.02–15 μM with equations of Ip = 2.0327C + 4.337 (R^2 = 0.9972), Ip = 1.777C + 3.7645 (R^2 = 0.9977) and Ip = 2.553C + 5.868 (R^2 = 0.9978), respectively. The LODs were determined using S/N = 3 to be 0.001, 0.0012, and 0.001 μM for MTBHQ, HQ, and CC, respectively.

3.8.3. Simultaneous detection

In this experiment for determination of MTBHQ, HQ and CC at ZnO@MnO_2-rGO/GCE, the concentration have increased simultaneously from 0.008 to 10 and 10 to 350 μM for MTBHQ, from 0.008 to 10 and 10 to 320 μM for HQ, from 0.008 to 8 and 8 to 330 μM for CC (Fig. 3a and b). The calibration equations for the detection of MTBHQ, HQ and CC were Ipa = 2.1305C + 6.112 (R2 = 0.9985, 0.008 to 10 μM), and Ipa = 0.2289C + 27.058 (R2 = 0.9982, 10 to 350 μM) for MTBHQ, Ipa = 1.9633C + 4.0546 (R2 = 0.9989, 0.008 to 10 μM) and Ipa = 0.1931C + 23.121 (R2 = 0.9979, 10 to 320 μM) for HQ, Ipa = 3.0785C + 6.3218 (R2 = 0.9987, 0.008 to 8 μM) and Ipa = 0.2799C + 31.1170 (R2 = 0.9982, 8 to 330 μM) for CC, and LODs were calculated based on 3S/N as 0.0011, 0.0012 and 0.001 μM for MTBHQ, HQ and CC, respectively (Fig. 3c). Comparing the equations obtained in the two experiments, it is clear that there is no change in the oxidation currents obtained in the experiments and it can be concluded that the analytes have no negative effect on each other's measurements.

3.9. Selectivity, repeatability, reproducibility, and stability studies

Several organic and inorganic substances are checked to test the selectivity of ZnO@MnO_2-rGO/GCE, as potential substances for the MTBHQ, HQ, and CC. The response of electrodes for oxidation of 3 μM MTBHQ, HQ, and CC were recorded in the absence and presence of foreign substances, and the level of change in oxide current was investigated. In these experiments, a species is selected as interference when the currents change ($\frac{\Delta I}{I} \times 100$, decreasing or increasing in oxidation current) are more than 5 %.

The investigation of the obtained data represents that the response of the ZnO@MnO_2-rGO/GCE for electro-oxidation of MTBHQ, HQ, and CC was not affected by common ions including Li^+, Mg^{2+}, Fe^{3+}, Cu^{2+}, Na^+, K^+, Cl^-, Zn^{2+}, NO^{3-}, Ca^{2+}, and SO_4^{2-} even in 250-fold.

Also, MTBHQ, HQ, and CC were detected simultaneously in the presence of typical interfering substances such as 50-fold excess concentration of Bisphenol A and Uric acid, 10-fold excess concentration of Citric acid, Ascorbic acid, 150-fold excess concentration of Folic acid, Aspirin, Codeine, Caffeine, 200-fold excess concentration of glucose, fructose, lactose, 5-fold excess concentration of resorcinol, nitrophenol and phenol, 350-fold excess concentration Ethanol and Methanol. With the proposed working electrode, there were only negligible changes in peak current for three analytes (maximum 4.35 %, 3.9 %, 4.1 % for MTBHQ, HQ, and CC, respectively) when interference species were present, indicating good selectivity.

The presented method was tested by performing a series of repetitive electrochemical measurements. There was excellent repeatability of the peak currents of 10 μM of MTBHQ, HQ, and CC measured over five continuous determinations, with the RSD% calculated to be 2.1, 1.9, and 2.6 %.

The reproducibility of the proposed sensor was investigated by independently fabricating five electrodes with similar material and process and calculation of RSD%. The RSD% were 3.5, 3.9, and 3.8 % for 10 μM of MTBHQ, HQ, and CC, respectively, indicating a trustworthy construction technique and acceptable reproducibility.

The stability of the sensor in long term was checked by consecutive measurements of 10 μM of MTBHQ, HQ, and CC with the one sensor. The first 72 h of signal monitoring showed no significant decreases in the sensors' signals, while only a 1 % drop in the currents was detected.

After two weeks of storage in the refrigerator at 4 °C and determination of analytes concentration every day, ZnO@MnO_2-rGO/GCE showed DPV responses of 95.3, 95.5, and 95.1 % of its initial voltammetric currents for MTBHQ, HQ, and CC, respectively. Based on the observations, the proposed sensor has acceptable long-term stability for measuring target analytes.

3.10. Real samples analysis

To appraise the validity of the proposed electrochemical sensor,

Table 1
Determination of the MTBHQ, HQ, and CC in different real samples.

Sample	Analyte	Added (μM)	Found (μM)	Recovery %	RSD %	HPLC
Soybean oil sample	MTBHQ	0	0.91	–	2.33	0.92
		10	11.01	101	3.10	10.87
		20	20.96	100.2	3.05	19.95
	HQ	0	0.88	–	2.41	0.91
		10	10.90	100.2	3.15	10.94
		20	20.84	99.8	3.46	20.85
	CC	0	ND*	–	–	ND
		10	10.02	100.2	2.85	10.08
		20	20.14	100.7	2.46	19.97
Tap water	MTBHQ	0	ND	–	–	ND
		10	10.10	101	3.14	10.00
		20	20.42	102.1	3.19	19.97
	HQ	0	ND	–	–	ND
		10	10.28	102.8	1.99	10.11
		20	20.62	103.1	2.83	20.05
	CC	0	ND	–	–	ND
		10	9.75	97.5	3.12	10.04
		20	19.73	98.6	2.67	20.64
River water	MTBHQ	0	ND	–	–	ND
		10	9.68	96.8	2.92	9.75
		20	19.72	98.6	3.71	20.11
	HQ	0	ND	–	–	ND
		10	10.14	101.4	3.02	10.09
		20	20.57	102.8	2.41	20.65
	CC	0	ND	–	–	ND
		10	9.86	98.6	2.05	9.84
		20	20.61	103	2.11	20.12
Orange juice	MTBHQ	0	ND	–	–	ND
		10	10.23	102.3	3.19	10.33
		20	19.69	98.4	3.42	20.88
	HQ	0	ND	–	–	ND
		10	10.23	10.2.3	2.91	10.08
		20	19.71	98.6	1.59	19.65
	CC	0	ND	–	–	ND
		10	10.26	102.6	2.22	10.15
		20	19.91	99.6	2.64	20.91

ND: Not Determination.

Table 2
Determination of the MTBHQ, HQ, and CC in polymer samples.

Polymer sample	Analyte	Added (μM)	Found (μM)	Recovery %	RSD %	HPLC
O 115	MTBHQ	0	0.008	–	3.11	ND
		10	10.03	100.1	3.24	10.02
		20	19.96	99.7	2.59	19.98
	HQ	0	0.009	–	3.25	ND
		10	10.12	101	3.42	10.13
		20	20.23	101	2.46	20.25
	CC	0	ND	–	–	–
		10	10.33	103.3	2.93	10.19
		20	20.45	102.2	3.11	20.56
I 211	MTBHQ	0	0.005	–	3.34	ND
		10	10.21	102	2.74	10.20
		20	20.45	102.2	2.91	20.72
	HQ	0	0.009	–	2.63	ND
		10	10.18	101.6	3.05	10.24
		20	20.16	100.7	3.09	20.33
	CC	0	ND	–	–	–
		10	10.14	101.4	2.99	9.96
		20	19.87	99.3	2.82	19.75
V 301	MTBHQ	0	0.005	–	3.11	ND
		10	10.04	100.2	2.96	10.19
		20	19.88	99.3	2.94	20.25
	HQ	0	0.009	–	1.56	ND
		10	10.09	100.7	1.94	10.11
		20	19.98	99.8	2.37	20.19
	CC	0	ND	–	–	–
		10	10.24	102.4	3.51	10.19
		20	20.68	103.4	3.07	19.87

ND: Not Determination.

MTBHQ, HQ, and CC in different real samples including Soybean oil samples, Water samples, Orange juice and Polymer samples were detected. The standard addition method was used to determine the target analytes in the real samples. As part of the methodology evaluation, we also performed a recovery test on the spiked real samples with different concentrations of MTBHQ, HQ, and CC. To further investigate and check the accuracy of the proposed method, the data obtained by the electrochemical method were compared with HPLC data. The obtained results are summarized in Tables 1 and 2. It can be seen that the percentage of recoveries for the determination of the analytes in the real samples ranges were from 96.8 % to 103.4 %. Also, the RSD percentages for five independent replicate measurements were calculated for each analyte. The tabled results demonstrate that the working electrode based on ZnO@MnO_2-rGO/GCE can detect MTBHQ, HQ, and CC in real samples with high repeatability, accuracy, and precision.

4. Conclusion

In the presented research for the first time, a highly repeatable and accurate sensor was developed for the selective and sensitive electrochemical monitoring of MTBHQ, HQ, and CC. In the first part of the work, a new ZnO@MnO2-rGO nanocomposite with acceptable electrocatalytic features was synthesized, and then it was used for modification of GCE. The fabricated sensor displays three LR from 0.008 to 10 μM and 10 to 350 μM for MTBHQ, 0.008 to 10 μM and 10 to 320 μM for HQ, 0.008 to 8 μM, and 8 to 330 μM for CC with a LODs of 0.0011, 0.0012 and 0.001 μM for MTBHQ, HQ and CC, respectively. The studies have shown that the proposed method has good selectivity, repeatability, reproducibility, and stability. The effect of forging substrates on the signal of ZnO@MnO_2-rGO/GCE was investigated and obtained data showed that the oxidation currents of three analytes have changed lower than 5 % in the presence of interferences. To evaluate the efficiency of the method, the target analytes were measured in different real samples. The obtained data including recovery percentage (close to 100 %) and RSD% (maximum 3.71 %) as well as a comparison of data with the HPLC method confirmed the high accuracy and precision of the method.

CRediT authorship contribution statement

Viyana Movahed: Writing – review & editing, Data curation, Investigation, Software. **Leila Arshadi:** Investigation, Resources, Formal analysis. **Mehrnaz Ghanavati:** Project administration, Supervision, Formal analysis, Resources. **Ehsan Mahdavi Nejad:** Investigation, Software, Writing – review & editing. **Zahra Mohagheghzadeh:** Writing – review & editing, Investigation, Software. **Mosayeb Rezaei:** Conceptualization, Data curation, Formal analysis, Investigation, Software, Writing – review & editing, Resources.

Declaration of Competing Interest

The authors declare that they have no known competing financial interests or personal relationships that could have appeared to influence the work reported in this paper.

Data availability

Data will be made available on request.

Appendix A. Supplementary data

Supplementary data to this article can be found online at https://doi.org/10.1016/j.foodchem.2022.134286.

References

Afkhami, A., Madrakian, T., Sabounchei, S. J., Rezaei, M., Samiee, S., & Pourshahbaz, M. (2012). Construction of a modified carbon paste electrode for the highly selective simultaneous electrochemical determination of trace amounts of mercury(II) and cadmium(II). *Sensors and Actuators B: Chemical, 161*(1), 542–548.

Anantha, M., Kumar, S. K., Anarghya, D., Venkatesh, K., Santosh, M., Kumar, K. Y., & Muralidhara, H. (2021). ZnO@ MnO2 nanocomposite modified carbon paste electrode for electrochemical detection of dopamine. *Sensors International, 2*, Article 100087.

Awang, M. S., Bustami, Y., Hamzah, H. H., Zambry, N. S., Najib, M. A., Khalid, M. F., … Abd Manaf, A. (2021). Advancement in Salmonella detection methods: From conventional to electrochemical-based sensing detection. *Biosensors, 11*(9), 346.

Bagheri, H., Afkhami, A., Khoshsafar, H., Rezaei, M., & Shirzadmehr, A. (2013). Simultaneous electrochemical determination of heavy metals using a triphenylphosphine/MWCNTs composite carbon ionic liquid electrode. *Sensors and Actuators B: Chemical, 186*, 451–460.

Bagheri, H., Hajian, A., Rezaei, M., & Shirzadmehr, A. (2017). Composite of Cu metal nanoparticles-multiwall carbon nanotubes-reduced graphene oxide as a novel and high performance platform of the electrochemical sensor for simultaneous determination of nitrite and nitrate. *Journal of Hazardous Materials, 324*, 762–772.

Bagheri, H., Shirzadmehr, A., & Rezaei, M. (2015). Designing and fabrication of new molecularly imprinted polymer-based potentiometric nano-graphene/ionic liquid/carbon paste electrode for the determination of losartan. *Journal of Molecular Liquids, 212*, 96–102.

Bagheri, H., Shirzadmehr, A., & Rezaei, M. (2016). Determination of copper ions in foodstuff products with a newly modified potentiometric carbon paste electrode based on a novel nano-sensing layer. *Ionics, 22*(7), 1241–1252.

Bagheri, H., Shirzadmehr, A., Rezaei, M., & Khoshsafar, H. (2018). Determination of tramadol in pharmaceutical products and biological samples using a new nanocomposite carbon paste sensor based on decorated nanographene/tramadol-imprinted polymer nanoparticles/ionic liquid. *Ionics, 24*(3), 833–843.

Balram, D., Lian, K.-Y., Sebastian, N., & Rasana, N. (2021). Ultrasensitive detection of cytotoxic food preservative tert-butylhydroquinone using 3D cupric oxide nanoflowers embedded functionalized carbon nanotubes. *Journal of Hazardous Materials, 406*, Article 124792.

Bendary, E., Francis, R., Ali, H., Sarwat, M., & El Hady, S. (2013). Antioxidant and structure–activity relationships (SARs) of some phenolic and anilines compounds. *Annals of Agricultural Sciences, 58*(2), 173–181.

Buledi, J. A., Ameen, S., Khand, N. H., Solangi, A. R., Taqvi, I. H., Agheem, M. H., & Wajdan, Z. (2020). CuO nanostructures based electrochemical sensor for simultaneous determination of hydroquinone and ascorbic acid. *Electroanalysis, 32*(7), 1600–1607.

Deng, P., Zhou, C., Wei, Y., Yue, X., Li, J., Yao, L., … He, Q. (2022). Salicylaldehyde functionalized chitosan for electrochemical sensitive sensor: Simultaneous determination of catechol and hydroquinone. *Journal of Electroanalytical Chemistry, 116506*.

Fan, L., Hao, Q., & Kan, X. (2018). Three-dimensional graphite paper based imprinted electrochemical sensor for tertiary butylhydroquinone selective recognition and sensitive detection. *Sensors and Actuators B: Chemical, 256*, 520–527.

George, J. M., Antony, A., & Mathew, B. (2018). Metal oxide nanoparticles in electrochemical sensing and biosensing: A review. *Microchimica Acta, 185*(7), 1–26.

Harshitha, B. T., Manjunatha, J. G., Pushpanjali, P. A., Karthik, C. S., Sandeep, S., Mallu, P., … Anwer, M. K. (2021). Efficient electrochemical determination of catechol with hydroquinone at poly (L-serine) layered carbon paste electrode. *ChemistrySelect, 6*(26), 6764–6772.

Hassan, K. M., Hathoot, A. A., Abo oura, M. F., & Azzem, M. A. (2018). Simultaneous and selective electrochemical determination of hydroquinone, catechol and resorcinol at poly(1,5-diaminonaphthalene)/glassy carbon-modified electrode in different media. *RSC Advances, 8*(12), 6346–6355.

Hosseini, F., Bahmaei, M., & Davallo, M. (2021). Electrochemical Determination of Propranolol, Acetaminophen and Folic Acid in Urine, and Human Plasma Using Cu2O–CuO/rGO/CPE. *Russian Journal of Electrochemistry, 57*(4), 357–374.

Ishack, S., & Lipner, S. R. (2022). Exogenous ochronosis associated with hydroquinone: A systematic review. *International Journal of Dermatology, 61*(6), 675–684.

Kalpana, V., & Devi Rajeswari, V. (2018). A review on green synthesis, biomedical applications, and toxicity studies of ZnO NPs. *Bioinorganic chemistry and applications, 2018*.

Kant, T., Shrivas, K., Dewangan, K., Kumar, A., Jaiswal, N., Deb, M., & Pervez, S. (2022). Design and development of conductive nanomaterials for electrochemical sensors: A modern approach. *Materials Today Chemistry, 24*, Article 100769.

Karimi-Maleh, H., Beitollahi, H., Kumar, P. S., Tajik, S., Jahani, P. M., Karimi, F., … Rouhi, J. (2022). Recent advances in carbon nanomaterials-based electrochemical sensors for food azo dyes detection. *Food and Chemical Toxicology, 112961*.

Karthika, A., Raja, V. R., Karuppasamy, P., Suganthi, A., & Rajarajan, M. (2020). A novel electrochemical sensor for determination of hydroquinone in water using FeWO4/SnO2 nanocomposite immobilized modified glassy carbon electrode. *Arabian Journal of Chemistry, 13*(2), 4065–4081.

Kathuria, D., Bhattu, M., Verma, M., & Billing, B. K. (2022). Chromatographic techniques for the analysis of organophosphate pesticides with their extraction approach: A review (2015–2020). *Analytical Methods*.

Khoshsafar, H., Bagheri, H., Rezaei, M., Shirzadmehr, A., Hajian, A., & Sepehri, Z. (2016). Magnetic carbon paste electrode modified with a high performance composite based on molecularly imprinted carbon nanotubes for sensitive determination of levofloxacin. *Journal of The Electrochemical Society, 163*(8), B422.

Kumar, N., Gajraj, V., Rameshbabu, R., Mangalaraja, R., Joshi, N. C., & Priyadarshi, N. (2022). Redox additive electrolyte assisted promising pseudocapacitance from strictly 1D and 2D blended structures of MnO2/rGO. *Materials Characterization, 111991*.

Li, X., Jiang, S., Li, J., Li, K., & Li, J. (2022). Highly dispersed manganese dioxide nanoparticles anchored on diatomite surface by sol–gel method and its performance on soybean meal-based adhesive. *Journal of Applied Polymer Science, 139*(9), 51719.

Li, X., Xu, X., Xia, F., Bu, L., Qiu, H., Chen, M., … Gao, J. (2014). Electrochemically active MnO2/RGO nanocomposites using Mn powder as the reducing agent of GO and the MnO2 precursor. *Electrochimica Acta, 130*, 305–313.

Mahmoudi, E., Hajian, A., Rezaei, M., Afkhami, A., Amine, A., & Bagheri, H. (2019). A novel platform based on graphene nanoribbons/protein capped Au-Cu bimetallic nanoclusters: Application to the sensitive electrochemical determination of bisphenol A. *Microchemical Journal, 145*, 242–251.

Movahed, H. R., Rezaei, M., & Mohagheghzadeh, Z. (2021). Construction of electrochemical sensor modified with molecularly imprinted polymer and rGO-Fe3O4-ZnO nanocomposite for determination of bisphenol A in polymers and water samples. *Analytical and Bioanalytical Chemistry Research, 8*(4), 453–466.

Nogales-Delgado, S., Guiberteau, A., & Encinar, J. (2022). Effect of tert-butylhydroquinone on biodiesel properties during extreme oxidation conditions. *Fuel, 310*, Article 122339.

Pajooheshpour, N., Rezaei, M., Hajian, A., Afkhami, A., Sillanpää, M., Arduini, F., & Bagheri, H. (2018). Protein templated Au-Pt nanoclusters-graphene nanoribbons as a high performance sensing layer for the electrochemical determination of diazinon. *Sensors and Actuators B: Chemical, 275*, 180–189.

Park, J., Kim, J., Min, A., & Choi, M. Y. (2022). Fabrication of nonenzymatic electrochemical sensor based on Zn@ ZnO core-shell structures obtained via pulsed laser ablation for selective determination of hydroquinone. *Environmental Research, 204*, Article 112340.

Pinnataip, R., & Lee, B. P. (2021). Oxidation chemistry of catechol utilized in designing stimuli-responsive adhesives and antipathogenic biomaterials. *ACS Omega, 6*(8), 5113–5118.

Ratnam, K. V., Manjunatha, H., Janardan, S., Naidu, K. C. B., & Ramesh, S. (2020). Nonenzymatic electrochemical sensor based on metal oxide, MO (M= Cu, Ni, Zn, and Fe) nanomaterials for neurotransmitters: An abridged review. *Sensors International, 1*, Article 100047.

Rezaei, M. (2016). An Au-Pd@MWCNT/graphene Modified Carbon Paste Electrode as a Novel Nano-Composite Sensor for the Trace Determination of Nitrite. *Analytical and Bioanalytical Electrochemistry, 8*(3), 287–303.

Rosida, E. M., Mulyasuryani, A., & Tjahjanto, R. T. (2017). Modification of screen printed carbon electrode (SPCE) with Fe3O4 for the determination of nitrite (NO2-) in squarewave voltammetry. *Molekul, 12*(2), 139–145.

Sebastian, N., Yu, W.-C., Balram, D., Al-Mubaddel, F. S., & Noman, M. T. (2022). Nanomolar detection of food additive tert-butylhydroquinone in edible oils based on novel ternary metal oxide embedded β-cyclodextrin functionalized carbon black. *Food Chemistry, 377*, Article 131867.

Shirzadmehr, A., Rezaei, M., Bagheri, H., & Khoshsafar, H. (2016). Novel potentiometric sensor for the trace-level determination of Zn2+ based on a new nanographene/ion imprinted polymer composite. *International Journal of Environmental Analytical Chemistry, 96*(10), 929–944.

Sipa, K., Brycht, M., & Skrzypek, S. (2018). The effect of the supporting electrolyte on the voltammetric determination of the veterinary drug nitroxinil. *Journal of Electroanalytical Chemistry, 827*, 21–26.

Tang, J., Li, J., Liu, T., Tang, W., Li, N., Zheng, S., … Song, C. (2022). N-doped TiO2–carbon composites derived from NH2-MIL-125 (Ti) for electrochemical determination of tert-butylhydroquinone. *Food Analytical Methods*, 1–10.

Vedpathak, A. S., Desai, M. A., Bhagwat, S., & Sartale, S. D. (2022). Green strategy for the synthesis of K+ Pre-inserted MnO2/rGO and its electrochemical conversion to Na-MnO2/rGO for high-performance supercapacitors. *Energy & Fuels, 36*(8), 4596–4608.

Vishwanath, M. S., Swamy, B. K., & Vishnumurthy, K. (2022). Electrochemical detection of bisphenol A in presence of catechol and hydroquinone at copper oxide modified carbon paste electrode. *Materials Chemistry and Physics, 289*, Article 126443.

Wang, C., Zhao, P., Zhang, L., Wang, Y., Fu, Q., Li, R., … Fei, J. (2022). Switched electrochemical sensor for hydroquinone based on rGO@ Au, monoclinic BiVO4 and temperature-sensitive polymer composite material. *Microchemical Journal, 179*, Article 107412.

Wi, S., Woo, H., Lee, S., Kang, J., Kim, J., An, S., … Park, B. (2015). Reduced graphene oxide/carbon double-coated 3-D porous ZnO aggregates as high-performance Li-ion anode materials. *Nanoscale research letters, 10*(1), 1–8.

Wu, F., Zhao, J., Han, D., Zhao, S., Zhu, R., & Cui, G. (2021). A three-electrode integrated electrochemical platform based on nanoporous gold for the simultaneous determination of hydroquinone and catechol with high selectivity. *Analyst, 146*(1), 232–243.

Zeinali, S., Khoshsafar, H., Rezaei, M., & Bagheri, H. (2018). Fabrication of a selective and sensitive electrochemical sensor modified with magnetic molecularly imprinted polymer for amoxicillin. *Analytical and Bioanalytical Chemistry Research, 5*(2), 195–204.

Zhang, L., Liu, H., Ruan, H., Su, Y., Hu, R., Tian, L., … Li, J. (2016). Fabrication of β-MnO2/RGO composite and its electrochemical properties. *Int. J. Electrochem. Sci, 11*, 10815–10826.

Zhang, W., Wang, R., Luo, F., Wang, P., & Lin, Z. (2020). Miniaturized electrochemical sensors and their point-of-care applications. *Chinese Chemical Letters, 31*(3), 589–600.

Zhao, J., Ma, Z., Qiao, C., Fan, Y., Qin, X., & Shao, G. (2022). Spectroscopic monitoring of the electrode process of MnO2@ rGO nanospheres and its application in high-performance flexible micro-supercapacitors. *ACS Applied Materials & Interfaces*.